

NASA CR-174,025

NASA-CR-174025  
19850002695

# A Reproduced Copy OF

NASA CR-174,025

Reproduced for NASA  
*by the*  
**NASA Scientific and Technical Information Facility**

**LIBRARY COPY**

1985 1985

LANGLEY RESEARCH CENTER  
LIBRARY NASA  
HAMPTON, VIRGINIA

DRP/LANGLEY

INTERACTIVE AIRCRAFT FLIGHT CONTROL AND  
AEROELASTIC STABILIZATION

NASA/Langley Research Center Grant-NAG-1-157

Semi-annual Report

1 May 1984 through 31 October 1984

(NASA-CR-174025) INTERACTIVE AIRCRAFT  
FLIGHT CONTROL AND AEROELASTIC STABILIZATION  
Semiannual Report, 1 May - 31 Oct. 1984  
(Purdue Univ.) 19 p HC A02/NF A01 CSCL 01C

N85-11003

Unclas  
G3/08 24348

Submitted by:

Dr. Terrence A. Weisshaar

Principal Investigator



SCHOOL OF AERONAUTICS AND ASTRONAUTICS

PURDUE UNIVERSITY

WEST LAFAYETTE, INDIANA 47907

November 1984

N85-11003

### Summary

This report covers research during the period 1 May 1984 through 31 October 1984. During this time, an analytical model has been used to study the problem of integrated control system/structural dynamic design. This model utilizes the traditional typical section lifting surface with a control surface attached in 2-D unsteady incompressible flow. The studies have as their purpose the examination of the use of the location of the elastic axis of the airfoil as a design variable in the search for an actively controlled configuration that has a specified flutter margin. Items of interest include the determination of flutter speed and divergence speed as functions of a nondimensional parameter,  $a_e$ , that measures the location (in semi-chords) of the elastic axis with respect to the airfoil midchord. All other parameters are fixed. The behavior of velocity root locus curves with changes in  $a_e$  is illustrated. Also shown is an example of the use of sensitivity derivatives to reposition poles of the open-loop system.

The behavior of the actively controlled or closed-loop system is also discussed. A set of examples are presented to indicate how the shear center parameter,  $a_e$ , affects the design of the controlled system. Cost function contours are presented as functions of design airspeed and shear center location. It is concluded that the cost function itself is not a guide to the "best" design where structural and control parameters are included. Future work will extend this research to include an airfoil with body freedom and an airfoil with directional stiffness. The ISAC program, now operational at Purdue, will be used to generate necessary data.

### Discussion

This report is divided into two parts. The first part demonstrates the capability of an analytical method to predict or estimate changes in eigenvalue roots or poles due to changes in system parameters. The mathematical techniques utilized are well-documented in the literature. However, such techniques must be implemented and validated as an initial step towards using analytical techniques for control/structural design optimization. The system under investigation is a typical section airfoil with a trailing edge control surface in 2-D unsteady incompressible flow, as shown in Figure 1. The airfoil is restrained by translational (plunge) and torsion (pitch) springs; the control surface is restrained by a torsion spring at its hinge point. The motion-dependent aerodynamic loads are represented by a series of exponential functions approximating the Wagner function from which are derived explicit expressions for the unsteady airloads in the time domain. The final form of the airloads has the form of Roger's approximation.

An airfoil, previously analyzed by Edwards using the generalized (s-plane) Theodorsen function, is used as a baseline configuration. The baseline parameters are listed in Table 1.

Table 1: Baseline Configuration

$\omega_a = 100 \text{ rad/sec}$	$\nu_c = 0.2$
$\omega_h = 50 \text{ rad/sec}$	$\nu_c \nu_\beta = 0.0125$
$\omega_\beta = 300 \text{ rad/sec}$	$a_e = -0.4$
$\mu = \frac{M}{4 b^2} = 10\pi$	$c = 0.6$
$r_\alpha = 0.5$	
$r_\beta = 0.079057$	

Figure 2 shows a comparison of root loci obtained from Edwards' analysis with root loci obtained with the present formulation (note that Edwards' root loci are "exact"). Each mode is labeled according to its "ancestry" (i.e. the dominant displacement at low airspeeds).

Figure 3 shows divergence and flutter speed boundaries as a function of the shear center position. The mass distributions and spring stiffnesses are held fixed. As a result, any parameters in Table 1 referenced to the shear center must be modified accordingly. The flutter boundary was determined by eigenvalue calculation, however, the divergence boundary was determined using the well-known formula for divergence of a 2-D typical section. Divergence on a root-locus plot is indicated by the crossing of an eigenvalue, corresponding to one of the "aerodynamic states", from the negative real axis to the positive real axis.

In Figure 3, a dashed line is labeled "Mode Transition". For shear center positions forward of this point ( $a_e \approx -0.263$ ), flutter occurs as an instability of the "bending" mode (as in Fig. 2). For shear center positions aft of this point, flutter appears as an unstable "torsion" mode. The flutter eigenvectors of these two modes themselves are similar, however, their root-locus "ancestries" differ.

The trajectories of the eigenvalues in the s-plane at selected airspeeds as shear center position changes, is depicted in Figure 4. The shear center root loci (solid lines) were determined by plotting airspeed root loci (long-dashed lines) for shear center positions ranging from a forward position of  $a_e = -0.5$  (i.e. at the 1/4 chord) to a farther aft position of  $a_e = -0.1$ . As  $a_e$  is increased from -0.5, the root loci approach the "Mode Transition" curves (short-dashed lines). At an  $a_e$  value of approximately -0.263 it is believed, though not demonstrated here, that the root loci are coincident

with these curves. The "Mode Transition" curves were determined by plotting root loci, as shown in Figure 5, for a large number of  $a_e$  and  $\bar{U}$  values. On the Mode Transition curves, as the "torsion" root descends and the "bending" root ascends, they meet at an airspeed parameter value between 6.0 and 6.5. At airspeed values beyond this point, the identities of the modes are ambiguous. As  $a_e$  is further increased, mode identities again become clear. However, the "bending" mode has changed from a flutter-critical mode to a highly damped mode. Conversely, the "torsion" mode has changed from a highly damped mode to a flutter-critical mode. It is uncertain whether this root locus behavior reflects a physical reality or is an artifice of the mathematics. However a similar mode transition is found in analytical studies of forward-swept-wing aircraft aeroelasticity.

This mode transition phenomenon poses problems if tracking mode ancestry is important to an analysis. An example of this difficulty, deliberately chosen to be pathological, is shown in Figure 6. Here, the initial value of  $a_e$  is chosen to be  $a_e = -0.3$ . The problem posed is the estimation of the root loci for  $a_e = -0.2$ . This example will involve, then, the mode transition difficulty. The eigenvalue sensitivity derivatives for  $a_e = -0.3$  are used in a first-order estimation of the eigenvalues for  $a_e = -0.2$  as follows:

$$\lambda_{\text{new}} \approx \lambda_{\text{old}} + \Delta\lambda = \lambda_{\text{old}} + \frac{\partial\lambda}{\partial a_e} \cdot \Delta a_e$$

The shear center position change,  $\Delta a_e = +0.1$ , is perhaps larger than is advisable in any circumstance, however, this large value permits a clearer demonstration.

In Figure 6, the initial root loci are shown, as are the estimated and actual root loci for the new shear center position. It is evident that substantial estimation errors occur around  $\bar{U} = 6.0$ . Note that, in Figure 4,

both the airspeed and shear center root loci tend to exhibit rather large curvatures in this region. The eigenvalues predicted beyond  $\bar{U} = 6.5$  (e.g. at  $\bar{U} = 7.0$ ) compare more favorably with the actual eigenvalues, even though they are of differing ancestries. Since much of the extreme curvature of the root loci is no longer present near the imaginary axis, the use of eigenvalue sensitivity derivatives to stabilize flutter roots, without regard to mode ancestry, should be acceptable.

Figures 7 and 8 depict examples of eigenvalue estimation for configurations with shear center parameters more removed from the mode transition region. Root loci curvatures are less severe and, hence, the linear estimation procedure is more accurate.

Further investigations will address an open-loop optimization of instability speeds using the eigenvalue sensitivity derivatives to arrive at the optimal value of  $a_e$  as indicated by the intersection of the flutter and divergence boundaries shown in Fig. 3. Also, studies will be made of an aircraft model, consisting of typical sections for the main wing and the canard/tail attached to a fuselage with pitch freedom. Both the airfoil and aircraft models will be used in studies of active control designs. The immediate objective of these studies will be to identify behavior patterns for these configurations, including any "pathological" conditions similar to the one described here, or entirely new ones.

### Combining Active Control with Structural Design

Recent efforts also have been directed toward examining the behavior of an actively controlled typical section airfoil, such as that previously discussed. Optimal linear regulator theory, in which a quadratic "cost" function  $J$  of the system state and control variables, integrated over infinite time, is minimized, is being used to determine full-state feedback gains for a trailing edge control surface actuator. Of particular interest are the effects on control law design of both shear center position and the airspeed at which the control laws are determined. The measure of these effects is the value of the minimized cost function,  $J$ , and the system stability boundaries.

A large number of cases were considered in which the optimal control of a 2-D airfoil at a specified design reduced airspeed  $\bar{U}_D (\bar{U} = \frac{U_\infty}{b} h)$  was determined. The variables in these studies were elastic axis position,  $a_e$ , and  $\bar{U}_D$ . In each case, a control law emerged. Shown in Figure 9 is a contour plot of the traditional cost function,  $J$ , for a range of shear center positions and design airspeeds (nondimensionalized as  $\bar{U} = \frac{U_\infty}{b} h$ ). Also shown are the open-loop flutter and divergence boundaries that exist before active control. At design speeds near  $\bar{U} = 6.5$  a very sharp cost increase develops with forward shear center locations ( $a_e < 0$ ). This particular design speed lies within the speed range for which the shear center root loci of the open-loop system lies within the mode transition region discussed previously. At lower airspeeds the shear center root loci associated with one characteristic mode remain associated with that mode. At higher airspeeds, although the shear center root loci associated with a particular mode cross the mode transition point, apparently continuously, they become dominated by the other mode. Whether or not these open-loop and closed-loop characteristics



associated with this airspeed are related is uncertain. There appears to be no correlation between the shear center position at which the open-loop mode transition occurs and the closed-loop behavior of the system.

Figure 10 shows stability boundaries for the baseline airfoil ( $a_e = -0.4$ ) as a function of design speed,  $\bar{U}_{\text{DESIGN}}$ . It is evident that the low costs associated with the lower design speeds in Figure 9 do not coincide with worthwhile improvements in stability. In fact there does not seem to be any airspeed at which a suitable active control design can be obtained when  $a_e = -0.4$ .

A markedly different situation results for control designs when a further aft position,  $a_e = -0.2$ , is used. In Figure 11, it is seen that flutter characteristics are improved somewhat at lower design airspeeds. In addition, flutter is eliminated at higher airspeeds without a drastic increase in the cost. Stability of the closed-loop system at a high design speed ( $\bar{U} = 9.5$ ) has also been investigated. This investigation reveals no flutter.

Figures 12a and 12b, show values of the dominant feedback gains, plotted as  $g$  versus design airspeed,  $\bar{U}$ . Figure 12a shows these gains for  $a_e = -0.4$  while Figure 12b illustrates these values for  $a_e = -0.2$ . Thus the shear center has moved aft in Figure 12b.

Figure 12a indicates the troublesome nature of the airspeed region near  $\bar{U} = 6.5$  when  $a_e = -0.4$ . The gains are much smaller when  $a_e = -0.2$ , but the gain,  $g_h$ , begins to increase rapidly when the design speed exceeds  $\bar{U} = 8.0$ .

From these limited results, it is obvious that structural design, as represented by the shear center position, can have a beneficial effect upon optimal control design for the closed-loop system, just as it does

upon open-loop system behavior. These results suggest that the use of the cost function,  $J$ , alone in an iterative redesign procedure may not always result in a desirable closed-loop system. Stability boundaries must also be considered.

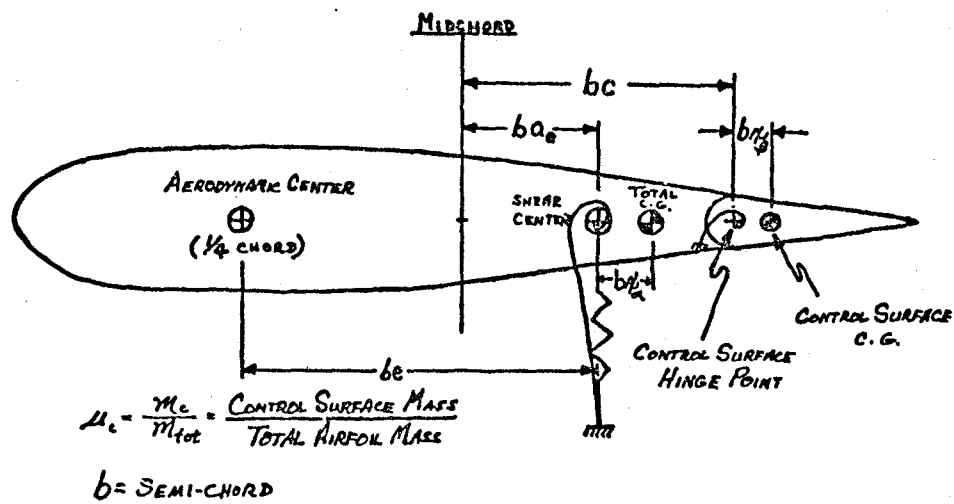


Figure 1 - Airfoil geometry.

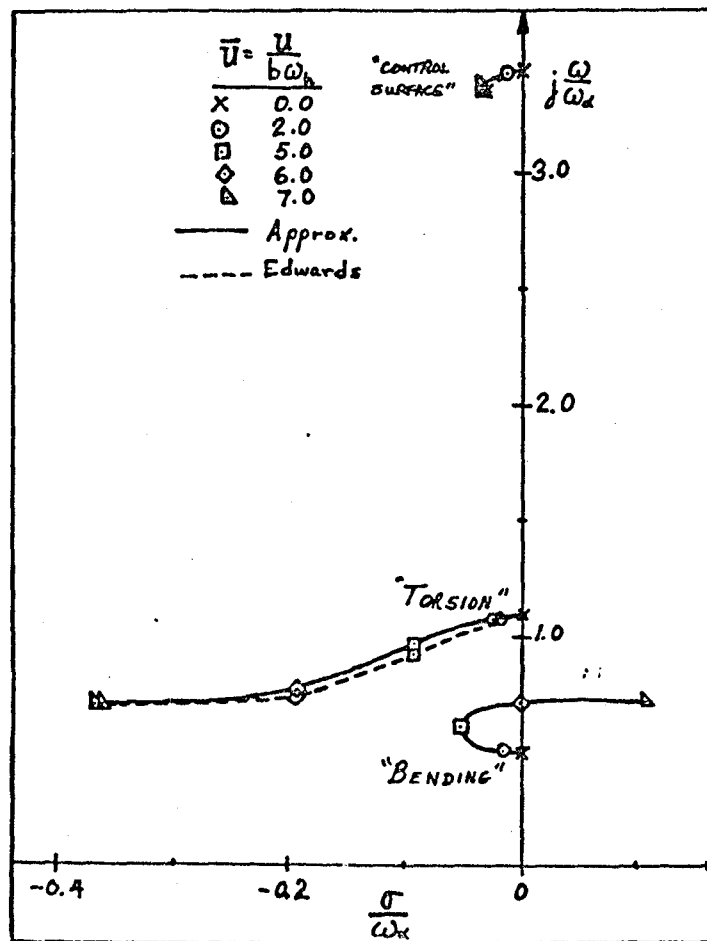


Figure 2 - Comparison of airspeed root loci for baseline Purdue configuration and Edwards Airfoil example.

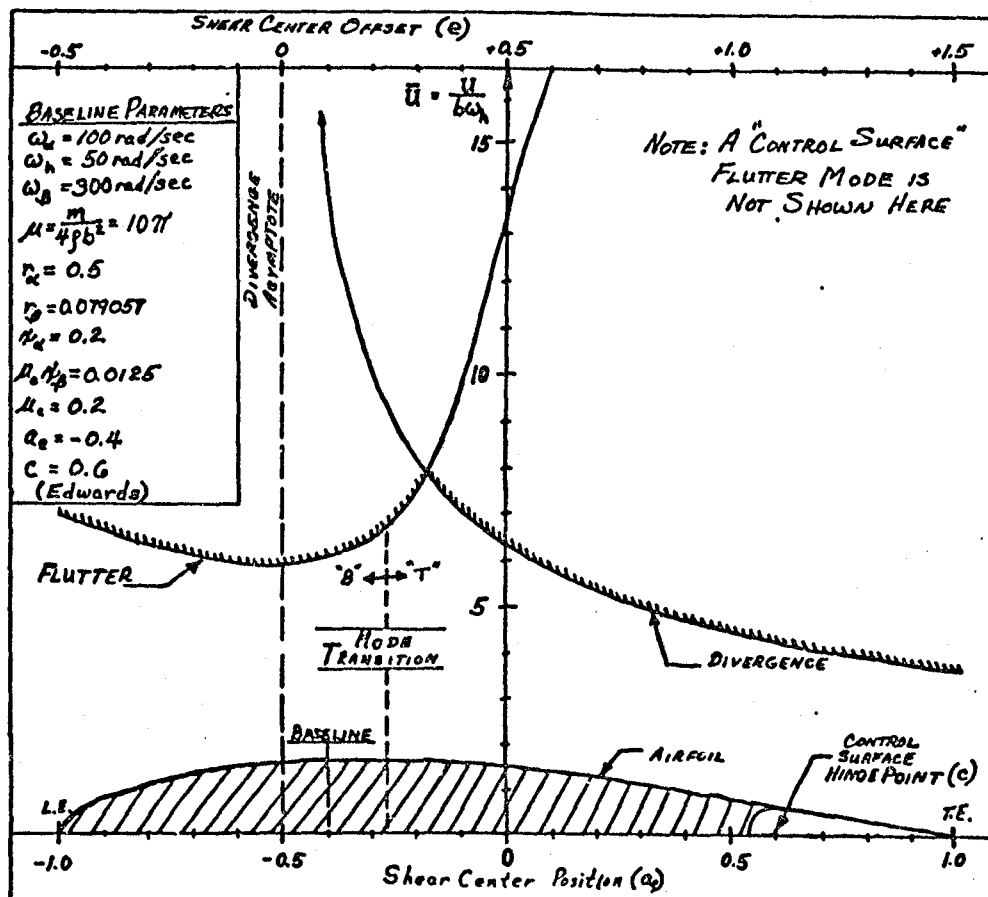


Figure 3 - Flutter and divergence stability boundaries as a function of shear center position,  $a_e$ .

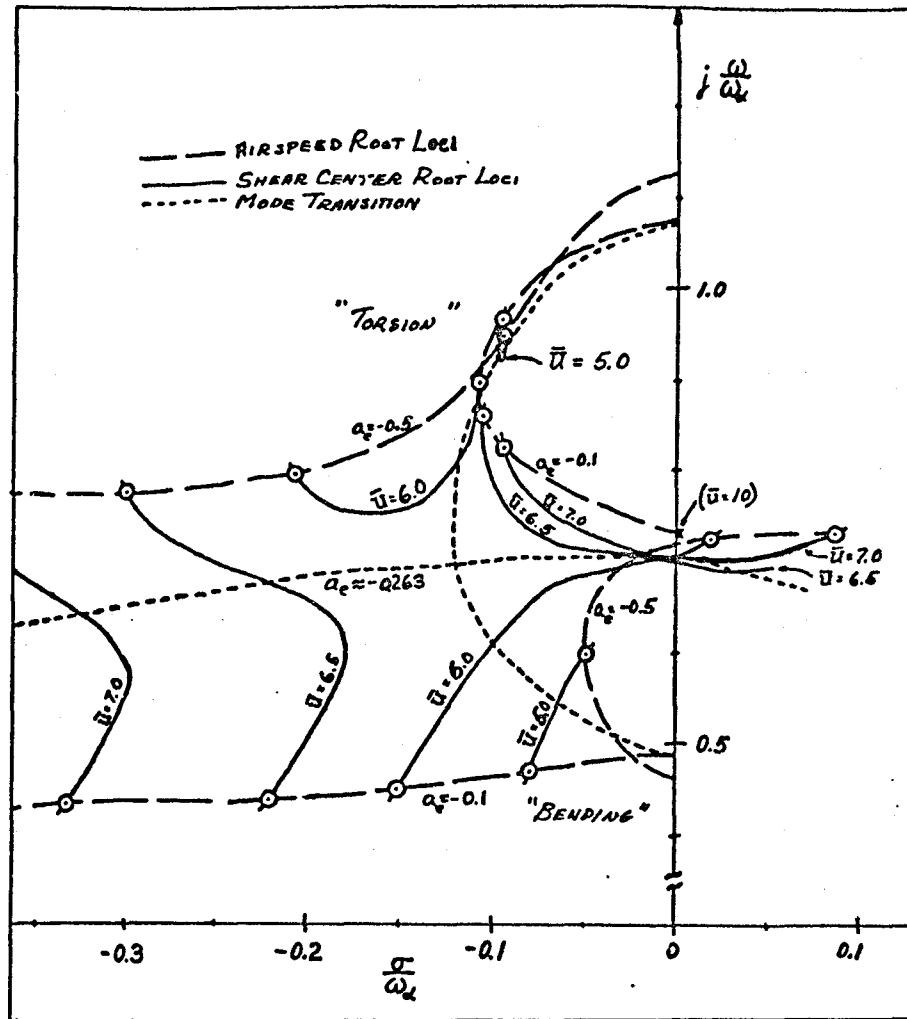


Figure 4 - Airspeed and shear center root loci for Purdue airfoil. Dashed lines indicate mode transition region.

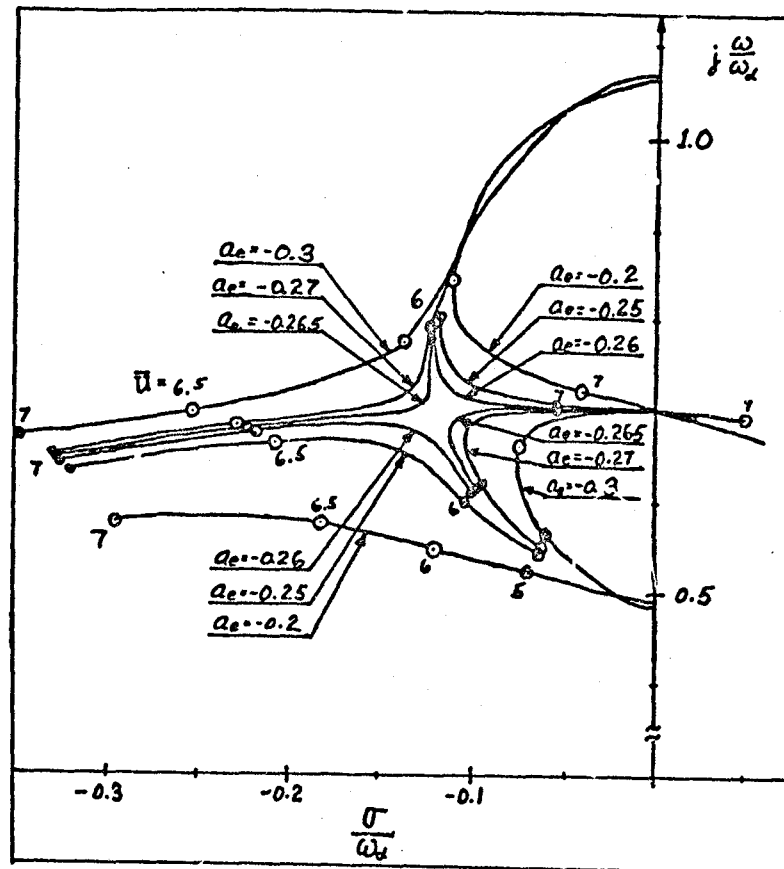


Figure 5 - Airspeed root locus curves for several shear center positions.

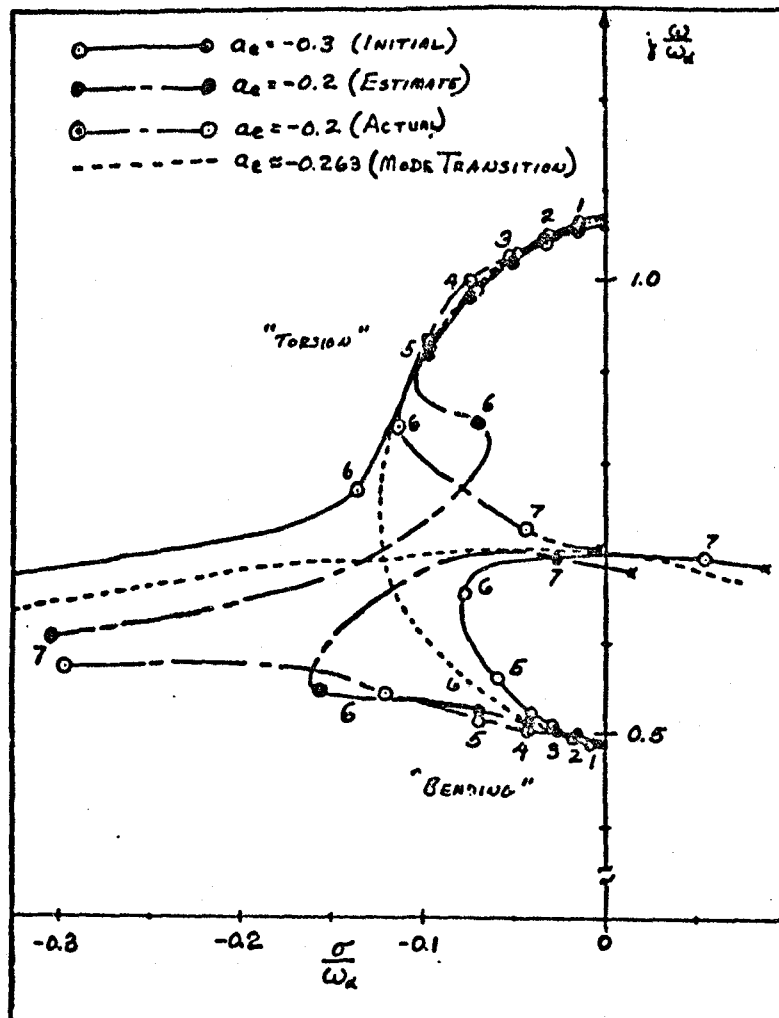


Figure 6 - Demonstration of root locus estimation procedure, with  $a_e$  as the parameter, at  $a_e = -0.3$ .

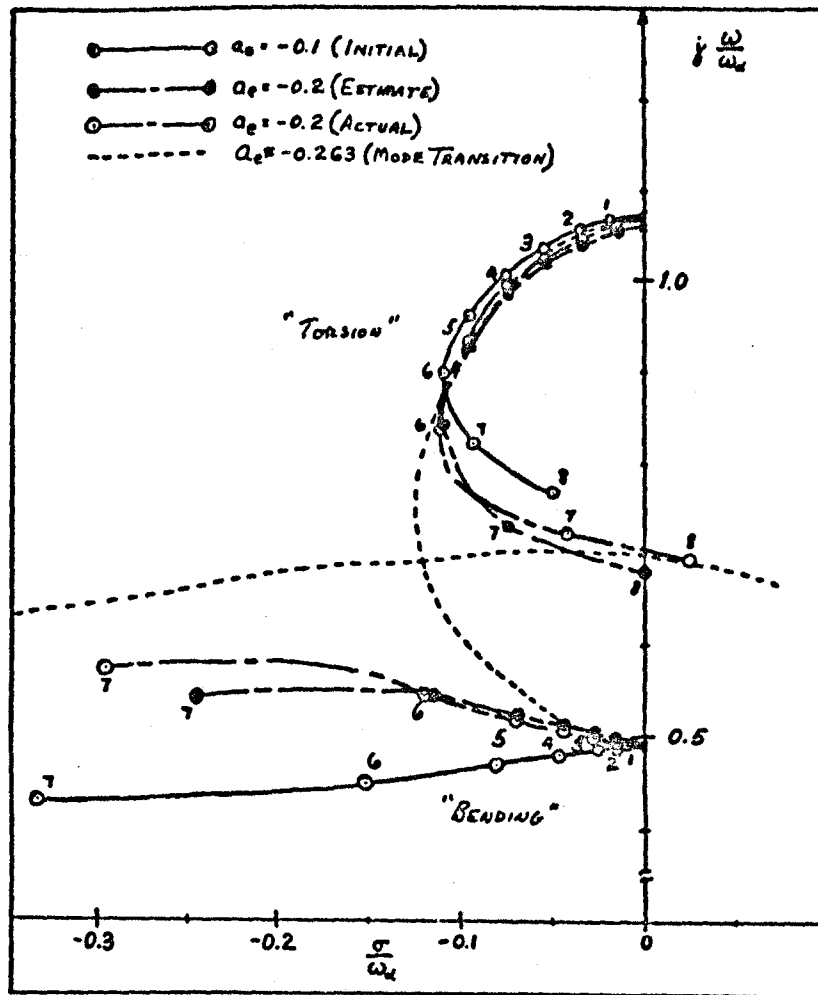


Figure 7 - Demonstration of root-locus estimation procedure at  $a_e = -0.1$ .



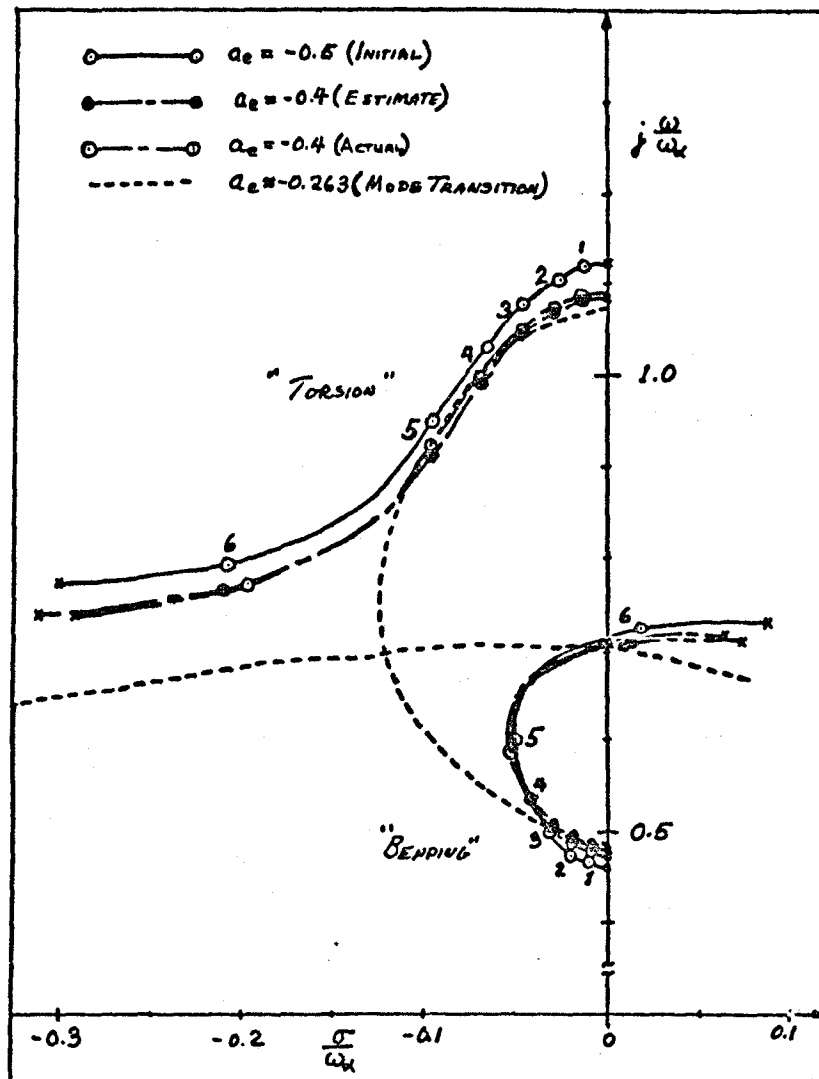


Figure 8 - Demonstration of root-locus estimation procedure at  $a_e = -0.5$ .

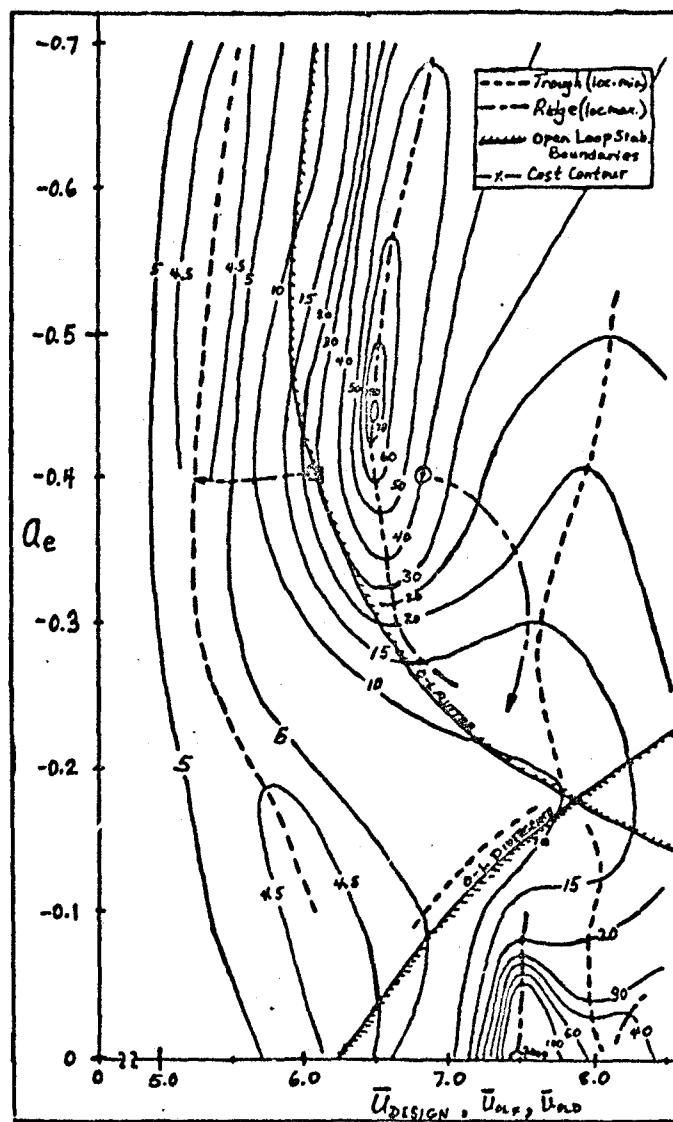


Figure 9 - Lines of constant optimal control cost,  $J$ , as a function of shear center position,  $a_e$ , and design airspeed,  $\bar{U}_D$ . Also shown are the open-loop (O-L) flutter and divergence boundaries.

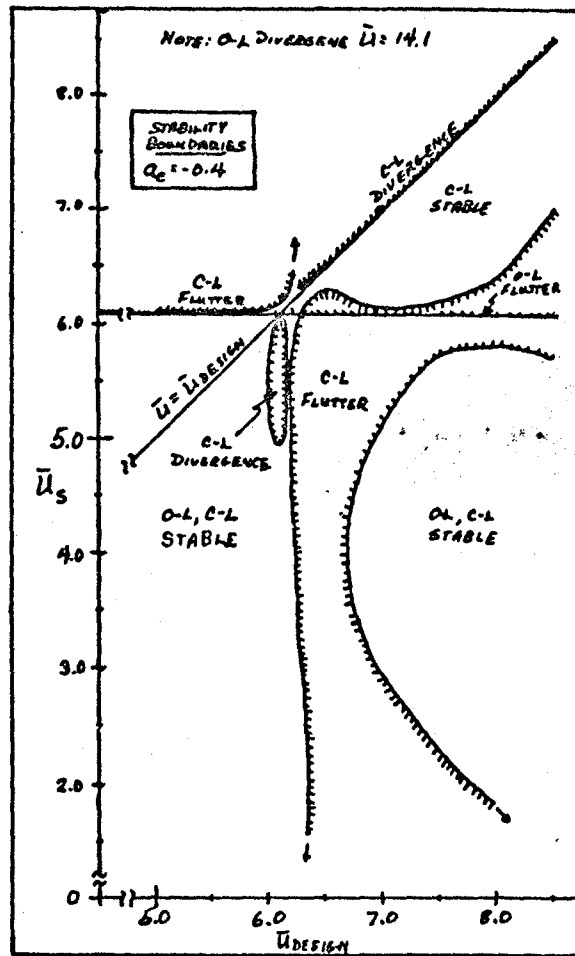


Figure 10 - Stability boundaries,  $\bar{U}_s$ , versus active control design airspeed,  $\bar{U}_D$ , for  $a_e = -0.4$ .

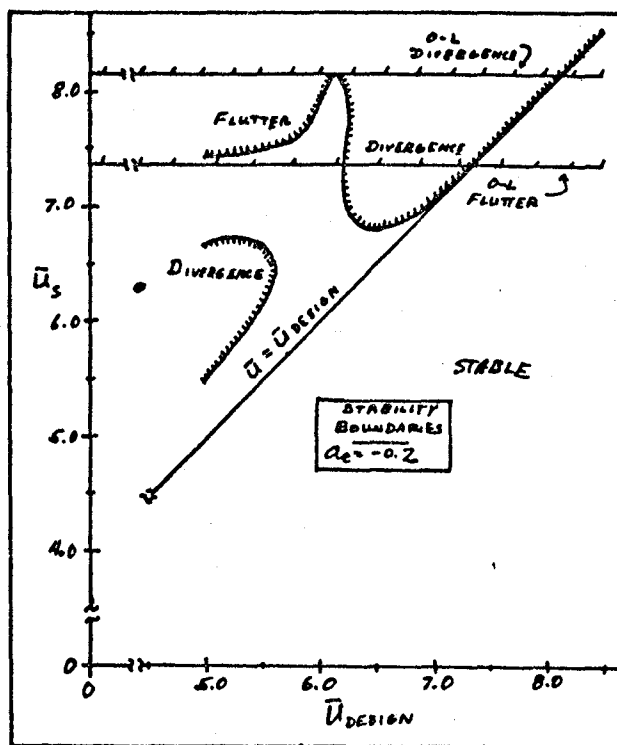


Figure 11 - Stability boundaries,  $\bar{U}_S$ , versus active control design airspeed,  $\bar{U}_D$ , for  $a_e = -0.2$ .

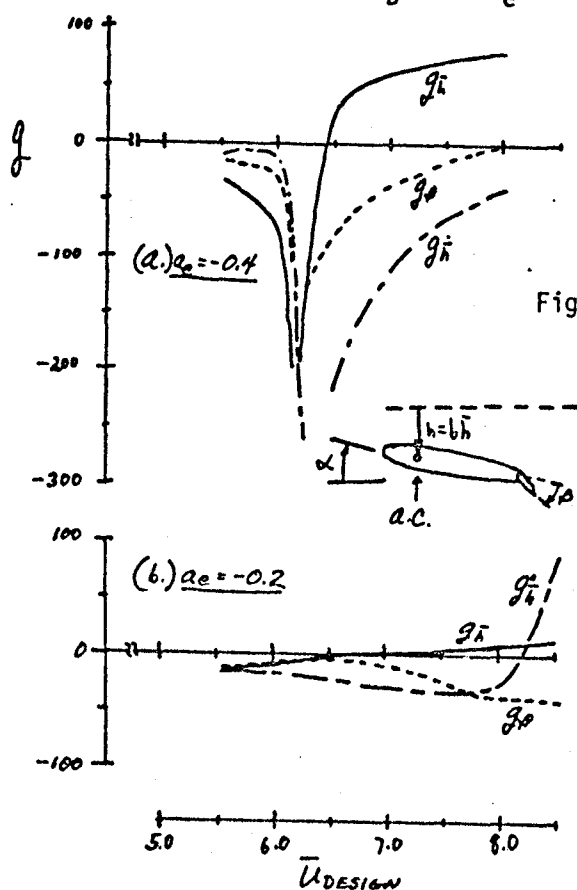


Figure 12 - Feedback gains  $g_{\bar{h}}$ ,  $g_{\dot{\bar{h}}}$ ,  $g_{\bar{p}}$  for

(a)  $a_e = -0.4$ , and

(b)  $a_e = -0.2$ .

**END  
DATE  
FILMED**

**JAN 15 1958**

LANGLEY RESEARCH CENTER



3 1176 00512 6975